The Astrophysical Journal, 591:962–967, 2003 July 10
© 2003. The American Astronomical Society. All rights reserved. Printed in U.S.A.

A TEST CASE FOR THE ORGANIC REFRACTORY MODEL OF INTERSTELLAR DUST

S. S. Shenoy,[1] D. C. B. Whittet,[1] J. E. Chiar,[2] A. J. Adamson,[3] W. G. Roberge,[1] and G. E. Hassel[1]
Received 2002 November 28; accepted 2003 March 18

ABSTRACT

The organic refractory model of interstellar dust postulates that the grains primarily responsible for visual extinction consist of silicate cores coated with organic refractory matter (ORM) supposed to form by photochemical processing of ice mantles. We identify the line of sight to the early-type star Elias 25, in the ρ Oph dark cloud, as a test for local production of ORM in an environment where mantled grains are exposed to a substantial ultraviolet radiation field. Infrared spectra of Elias 25 in the 2.4–4.0 μm region were used to examine the 3 μm ice profile and to search for the C—H bond absorption feature near 3.4 μm that occurs in laboratory-synthesized ORM. We find that the ice feature in Elias 25 has an unusually deep 3.1–3.7 μm wing, but no detectable 3.4 μm feature is present in the wing profile. An upper limit on the $\tau_{3.4}/A_V$ ratio is set that is a factor of 4 lower than that determined from the feature detected in the diffuse interstellar medium toward Cygnus OB2 No. 12. Our results are consistent with other evidence indicating that the carrier of the 3.4 μm feature is destroyed, rather than produced, inside dense clouds.

Subject headings: astrochemistry — dust, extinction — infrared: ISM — ISM: lines and bands — ISM: molecules — stars: individual (Elias 25)

1. INTRODUCTION

One of the principal models for interstellar dust postulates that visual extinction is produced primarily by grains composed of silicate cores coated with mantles of organic refractory matter (ORM) (Hong & Greenberg 1980; Li & Greenberg 1997). ORM is presumed to form by photochemical processing of the ice mantles that grow on the surfaces of dust grains in molecular clouds, a mechanism that has been verified experimentally for laboratory analogs (e.g., Briggs et al. 1992; Strazzulla & Baratta 1992; Jenniskens et al. 1993; Greenberg et al. 1995). Species such as H_2O, NH_3, CO_2, CH_3OH, and CH_4 present in the ices are converted into radicals, and subsequent reactions produce species of higher molecular weight. The end products contain both aromatic groups and aliphatic chains, resembling kerogens and other complex organic moieties found in carbonaceous meteorites (de Vries et al. 1993). The production mechanism is presumed to operate in the vicinity of embedded, young stellar objects (YSOs) that form within the clouds, especially massive YSOs that generate strong ultraviolet (UV) photon fluxes as they approach the main sequence. Recently, Gibb & Whittet (2002) presented spectral evidence consistent with ORM production in the envelopes of certain massive YSOs. If ORM is a widespread component of interstellar dust in the general interstellar medium, however, it must be produced efficiently throughout star formation regions exposed to significant UV flux, and not merely in the circumstellar envelopes of a few massive objects.

Laboratory-synthesized ORM displays several infrared spectral signatures, including a C—H stretching feature at 3.4 μm, together with overlapping features in the 5–10 μm region attributed to a variety of vibrational modes (Greenberg et al. 1995; Pendleton & Allamandola 2002): of the latter, the carbonyl (C═O) feature near 6 μm provides a particularly sensitive diagnostic of ORM (Pendleton & Allamandola 2002; Gibb & Whittet 2002), but studies of this spectral region are currently limited to bright sources observed with existing space or airborne instruments. Ground-based studies are feasible only for the C—H feature at 3.4 μm. An interstellar 3.4 μm feature is, indeed, observed in lines of sight that intercept significant columns of diffuse (low-density) interstellar medium (ISM), and this is similar in both position and profile shape to absorptions in the laboratory analogs. It should be noted, however, that the observed 3.4 μm feature is not identified unambiguously with ORM produced in the manner described above; it could also arise, for example, in short aliphatic hydrocarbon chains attached to small amorphous carbon grains that might form in C-rich stellar outflows (Sandford et al. 1991; Tielens et al. 1994; Chiar et al. 1998; Mennella et al. 1999; Schnaiter et al. 1999; Pendleton & Allamandola 2002). In denser clouds, this part of the spectrum is confused by the presence of the broad 2.8–3.7 μm H_2O ice feature. Detailed profile studies have found no evidence for a 3.4 μm counterpart to the diffuse ISM feature in the wing of the ice feature (Allamandola et al. 1992; Brooke, Sellgren, & Smith 1996; Brooke, Sellgren, & Geballe 1999; Chiar, Adamson, & Whittet 1996; Muñoz Caro et al. 2001). Instead, a smooth feature centered at 3.47 μm is observed, tentatively attributed to hydrocarbons in icy mantles (Allamandola et al. 1992; Brooke et al. 1996; Chiar et al. 1996; Grishko & Duley 2000). This might be understood if the 3.4 μm carriers are selectively destroyed or chemically altered inside dark clouds, where grains are subject to growth by both coagulation and mantle deposition. However, if molecular clouds containing newly formed stars are the production sites for organic refractory mantles, then we should expect to find spectral evidence for them there.

As a test of ORM production, we present in this paper a search for 3.4 μm absorption toward the B-type zero-age

[1] Department of Physics, Applied Physics and Astronomy, and New York Center for Studies on the Origins of Life, Rensselaer Polytechnic Institute, Troy, NY 12180.

[2] NASA Ames Research Center, Mail Stop 245-3, Moffett Field, CA 94035; and SETI Institute, 2035 Landings Drive, Mountain View, CA 94043.

[3] Joint Astronomy Centre, 660 North A'ohoku Place, University Park, Hilo, HI 96720.

main-sequence star Elias 25 in the ρ Oph dark cloud (Elias 1978). The ρ Oph cloud is a suitable test case because it combines a strong UV field with a relatively dense environment in which grains are known to have ice mantles at moderate to high optical depth (Tanaka et al. 1990). Elias 25 is known to be embedded in the dense cloud as it illuminates faint nebulosity, displays a shallow ice feature, and suffers much higher total extinction ($A_V \approx 12.5$ mag) than could reasonably arise in ambient interstellar dust. Dust in the line of sight is characterized by elevated values of the ratio of total to selective extinction ($R_V = A_V/E_{B-V} \approx 4.3$) and the wavelength of maximum polarization ($\lambda_{\max} \approx 0.66$ μm) compared with the diffuse ISM averages of 3.1 and 0.55 μm, respectively (Whittet et al. 1992). Increases in R_V and $\lambda_{\max}$ provide evidence for grain growth, most likely the result of coagulation (Jura 1980; Vrba, Coyne, & Tapia 1993). One effect of coagulation is to reduce the UV extinction per unit A_V (because the small grains responsible for UV extinction become depleted), thus moderating the degree of attenuation of the stellar UV radiation field within the cloud (see Bohlin & Savage 1981; Cecchi-Pestellini, Aiello, & Barsella 1995). The radiative environment of the region has been modeled in detail by Liseau et al. (1999). These authors deduce that the local radiation field, integrated over energies $6 \leq h\nu \leq 13.6$ eV, is typically a factor of 20–140 higher than the interstellar average, a finding attributed primarily to the presence of the nearby B2 V star HD 147889.

Section 2 describes the observations and data reductions. Our attempts to extract the 3.4 μm feature are described in § 3, and our results and conclusions are presented in § 4.

2. OBSERVATIONS AND DATA REDUCTIONS

Our target source was first detected by Grasdalen, Strom, & Strom (1973, their source 1), the designation Elias 25 arising from its inclusion in the catalog of 2 μm Ophiuchus sources published by Elias (1978). The infrared source corresponds to a faint ($V = 17.0$) visible star classified B3–5 V (Grasdalen et al. 1973; Vrba et al. 1975; Elias 1978). Spectra of Elias 25 and a standard star (HD 145100) were obtained with the United Kingdom Infrared Telescope (UKIRT) at Mauna Kea Observatory, Hawaii, during a service observing run on UT 2002 March 10. The stars were observed with CGS4, a cryogenically cooled grating spectrometer with a 256×256 InSb detector array. Spectral coverage from 2.4 to 4.0 μm was obtained in three overlapping segments centered at 2.699, 3.101, and 3.650 μm. The 40 line mm^{-1} grating was used in the first order with a 1 pixel slit width (corresponding to $0''.6$ pixel^{-1}), resulting in a mean resolving power $\lambda/\Delta\lambda \sim 1200$. The integration time in each wavelength band was 48 s.

All the data reduction was done using STARLINK FIGARO routines. During observation the source was nodded $\sim 12''$ along the slit for background subtraction. The spectra were oversampled by stepping the detector array in four steps over two resolution elements. This procedure introduces ripples in the spectra, because of transparency variations between array settings, which were removed successfully using the IRFLAT routine. The wavelength calibration was achieved using an argon arc lamp in the second order. The program star spectrum was ratioed by the standard star spectrum to eliminate telluric features. Flux calibration was then accomplished by multiplying the ratioed spectrum by a blackbody of temperature ($T = 6680$ K) appropriate to the standard star and scaling with respect to catalog magnitudes.

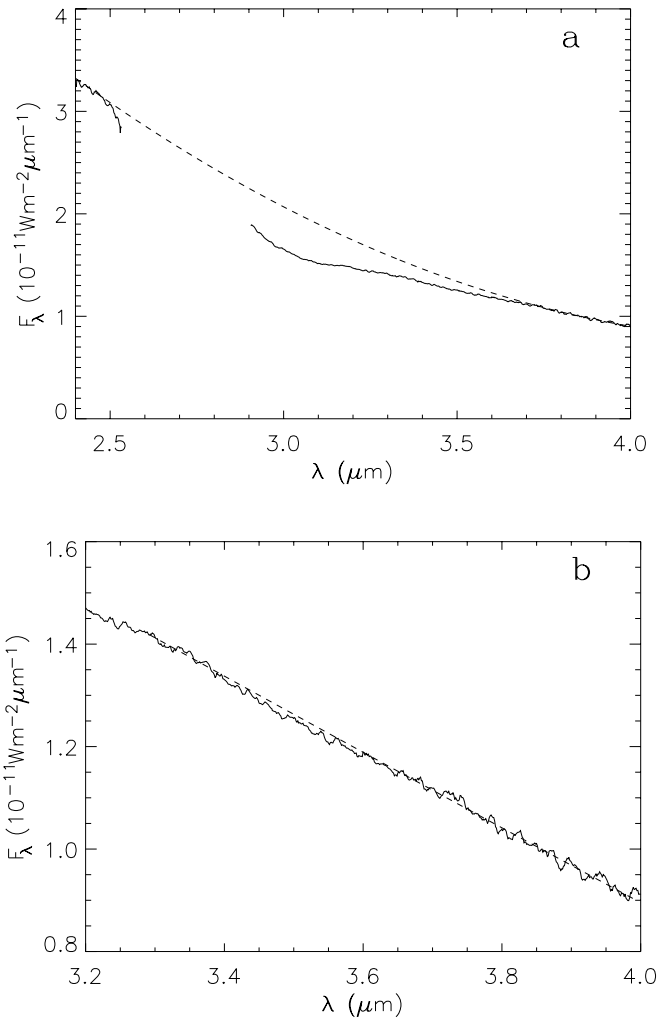


FIG. 1.—Calibrated flux spectrum of Elias 25. (*a*) The entire 2.4–4.0 μm spectrum, together with the second-order polynomial continuum (*dashed curve*) assumed for the 3.1 μm ice feature. The continuum is fitted to the spectrum in the wavelength ranges 2.4–2.5 μm and 3.8–4.0 μm. (*b*) The 3.2–4.0 μm section of the spectrum, together with the second-order polynomial "local" continuum (*dashed curve*) assumed for the 3.4 μm C—H feature. The continuum is fitted to the spectrum in the wavelength ranges 3.28–3.33 μm and 3.7–4.0 μm.

The final calibrated spectrum is shown in Figure 1*a* (full spectral coverage) and Figure 1*b* (enlargement of the 3.2–4.0 μm segment). Data in the 2.55–2.85 μm region of high telluric opacity are omitted from Figure 1*a*.

3. IN SEARCH OF THE 3.4 μm FEATURE

If present, the 3.4 μm feature will appear as weak structure in the long-wavelength wing of the H_2O ice feature (which extends approximately from 3.2 to 3.7 μm). We therefore begin by examining the ice profile. A continuum was fitted to the flux spectrum using the FIGARO ABLINE routine, as shown in Figure 1*a*. We used a second-order polynomial constrained at 2.4–2.5 and 3.8–4.0 μm. The derived optical depth spectrum, shown in Figure 2, is dominated by the ice feature. The peak optical depth of the feature is estimated to be $\tau_{3.1} = 0.23 \pm 0.01$, a result consistent

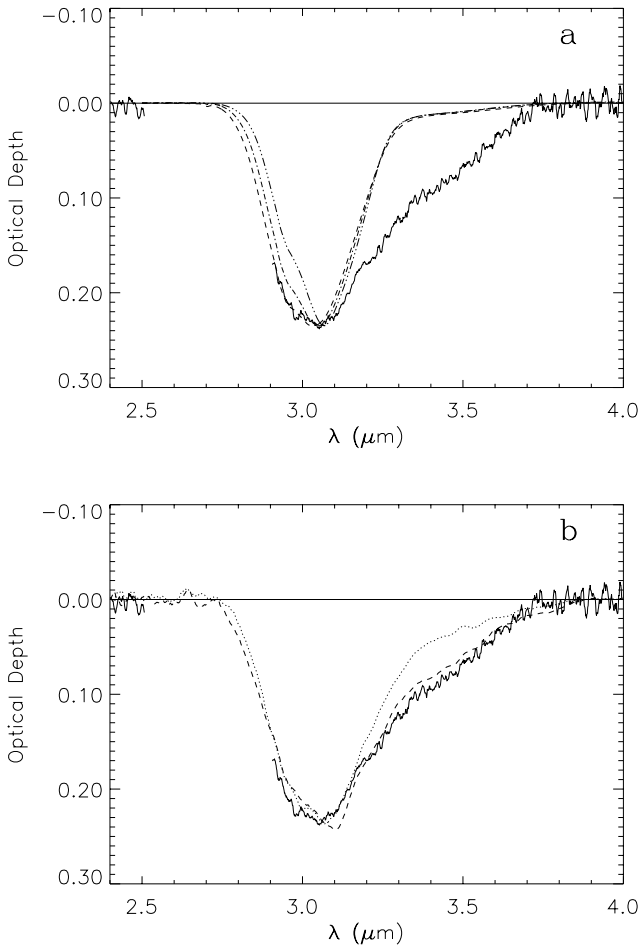


FIG. 2.—Optical depth spectrum of Elias 25 obtained using the continuum shown in Fig. 1*a*. (*a*) Comparison with data for a laboratory $H_2O:NH_3$ ice at three different temperatures: 10 K (*dashed curve*), 50 K (*dash-dotted curve*), and 80 K (*dash–double-dotted curve*). In each case, the laboratory spectrum is scaled to the peak optical depth of the observed ice feature at 3.07 μm. (*b*) Comparison with observed profiles in two young stellar objects: Elias 29 (*dotted curve*) and AFGL 2591 (*dashed curve*), scaled to the 3.07 μm optical depth in Elias 25. Data for Elias 29 and AFGL 2591 are from the *ISO* SWS archive.

with an earlier determination by Tanaka et al. (1990). To illustrate the contribution of the wing to the ice profile in Elias 25, the observed optical depth spectrum is compared in Figure 2*a* with data for a laboratory ice composed of $H_2O:NH_3$ in the ratio 100 : 9 (taken from the University of Leiden Laboratory Astrophysics database). Spectra for three ice temperatures are shown (10, 50, and 80 K). We see that the short-wavelength side of the feature is well matched by 10 K ice, but none match the long-wavelength side. Indeed, no laboratory ice analog produced to date has succeeded in reproducing the long-wavelength wing.

The long-wavelength wing appears to be exceptionally deep in Elias 25. To illustrate this, the optical depth spectrum is compared in Figure 2*b* with data for two young stellar objects (YSOs) observed by the *ISO* Short Wavelength Spectrometer (SWS). We selected Elias 29 as the best-studied example of a YSO in the ρ Oph dark cloud (Boogert et al. 2000, 2002), and AFGL 2591 as a source with one of the deepest 3.2–3.7 μm wings in the *ISO* SWS spectral catalog (Gibb et al. 2003, in preparation). In both cases, the optical depth has been scaled to that of Elias 25 at the center of the ice feature. It is evident in Figure 2*b* that the "wing-to-trough" ratio of the ice feature is similar, comparing Elias 25 and AFGL 2591, and substantially lower in Elias 29. Source-to-source variations in the relative depth of the wing have been reported before (e.g., Smith, Sellgren, & Tokunaga 1989; Tanaka et al. 1990). Our results are in qualitative agreement with those of Tanaka et al., who find that the wing appears to deepen toward more evolved YSOs (emission-line objects) and early-type stars compared with protostars.

Two distinct approaches to the problem of extracting the putative 3.4 μm feature from the wing of the ice profile were adopted, following previous work by Brooke et al. (1999) and by Muñoz Caro et al. (2001). We refer to these as method 1 and method 2, respectively.

In method 1, we adopt a local continuum and attempt to identify the feature in the residual. The local continuum was chosen to be a second-order polynomial fit constrained at 3.28–3.33 and 3.7–4.0 μm, as shown in Figure 1*b*. The residual optical depth spectrum is plotted in Figure 3*a*. Although the vertical placement of the spectrum is sensitive to the choice of continuum, the presence or absence of structure should not be affected. The spectrum contains a weak ($\tau \sim 0.01$) absorption that peaks at 3.47 μm, i.e., at significantly longer wavelength than the 3.4 μm diffuse ISM feature. The sharp onset of the latter feature at 3.35–3.40 μm is its most easily distinguishable fingerprint, and there is no hint of this in Figure 3*a*. In Figure 3*b*, we compare the observed profile in Elias 25 with that of the prototypical diffuse ISM line of sight Cyg OB2 No. 12 (Whittet et al. 1997, 2001b). Figure 3*b* confirms that the feature in Elias 25 is different in both position and shape from the diffuse ISM feature. Absorption at 3.47 μm is associated with material in the ice mantles (§ 1): as Elias 25 has a modest ice feature, the presence of weak 3.47 μm absorption is not therefore unexpected. We modeled this feature, as outlined by Brooke et al. (1999), as a Gaussian with central wavelength $\lambda_0 = 3.469$ μm and width (FWHM) = 0.105 μm (Fig. 3*a*). After scaling and subtracting the modeled feature from the optical depth plot, we obtain the residual shown in Figure 3*c*. On the basis of this residual, we deduce that no counterpart to the 3.4 μm diffuse ISM feature is discernible: the degree of scatter in the data implies an upper limit $\tau_{3.4} < 0.01$ on the strength of the feature along the line of sight to Elias 25.

In method 2, following Muñoz Caro et al. (2001), we investigate the effect of subtracting a diffuse ISM 3.4 μm profile from the observed spectrum of Elias 25, as illustrated in Figure 4. Cyg OB2 No. 12 was chosen to represent the diffuse ISM. In Figure 4*a*, the dotted curve is the optical depth spectrum of Elias 25 (as Fig. 2*a*), and the solid curves are composites resulting from subtraction of the Cyg OB2 No. 12 spectrum with various scaling factors, such that the peak optical depth at 3.4 μm in Cyg OB2 No. 12 is 0.02, 0.04, . . ., 0.12. An appropriate choice of scale will result in elimination of the 3.4 μm feature in Elias 25. If, on the other hand, if we choose too large a scale, the feature will be overcompensated and will introduce "emission" structure in the spectrum. It is clear from inspection of Figure 4*a* that structure is least for scales of zero or 0.02. As a further constraint, we examine the behavior of the substructure centered near 3.48 μm present in the diffuse ISM profile (note that this is narrower than and distinct from the 3.47 μm substructure in the wing in the ice feature). We measured the strength of the

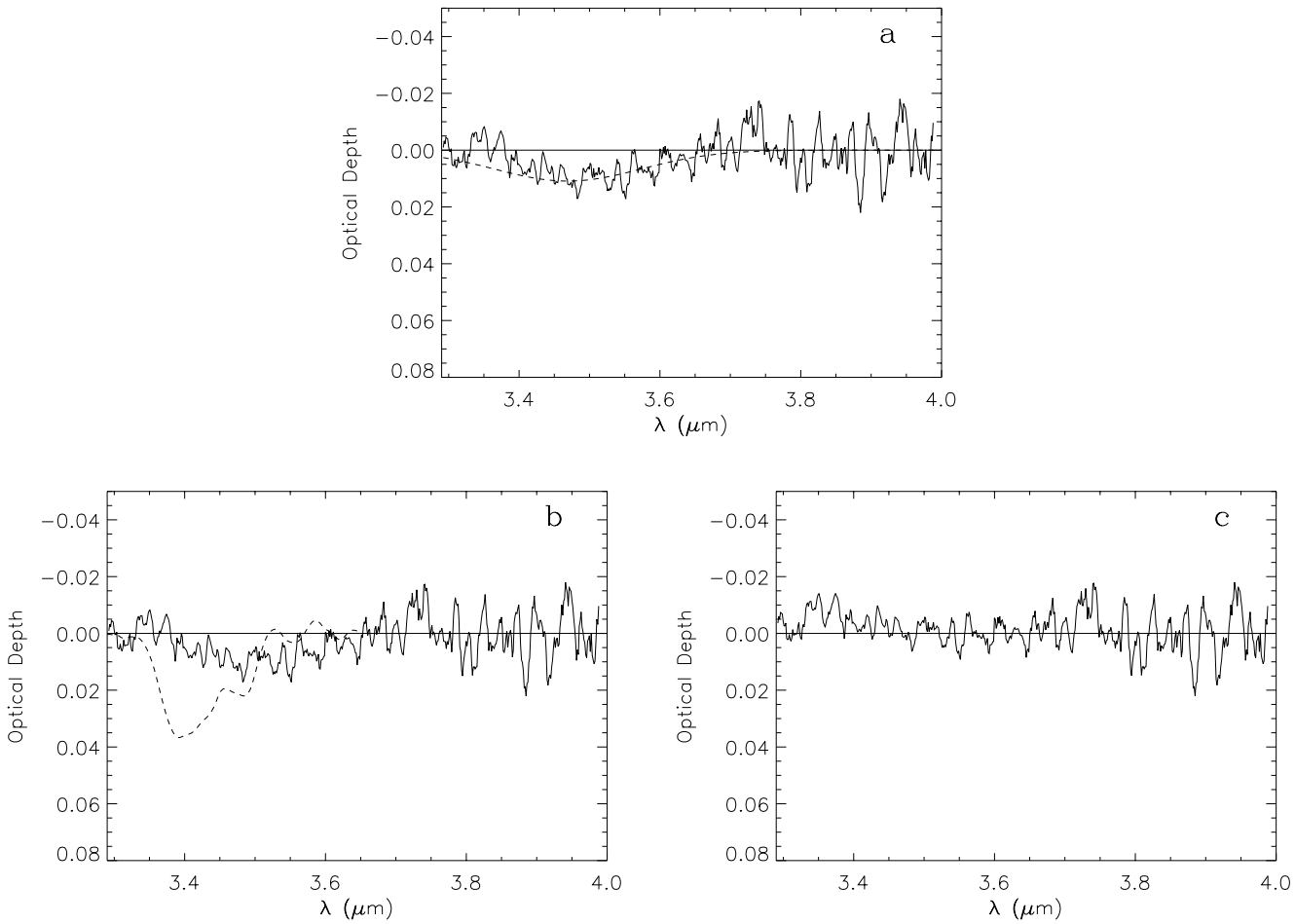


FIG. 3.—Optical depth spectrum of Elias 25 obtained using the continuum shown in Fig. 1*b*. (*a*) A fit to the weak absorption feature centered at 3.47 μm is shown (*dashed curve*), assuming it to be Gaussian, centered at 3.469 μm, and 0.105 μm in width (FWHM). (*b*) The spectrum of Elias 25 is compared with the 3.4 μm profile in Cyg OB2 No. 12 (*dashed curve*; *ISO* SWS data). (*c*) Residual optical depth after subtracting the Gaussian shown in (*a*) from the spectrum of Elias 25.

3.48 μm feature relative to a linear baseline fit to two peripheral regions of each composite spectrum (Fig. 4*a*, *vertical dashed lines*) and plotted this against the scaling factor in Figure 4*b*. From Figure 4*b*, we see that zero strength occurs at a scaling of 0.00 ± 0.01. From this we deduce that method 2 gives a result entirely consistent with method 1, i.e., $\tau_{3.4} < 0.01$.

4. DISCUSSION AND CONCLUSIONS

The principal result of this paper is that the 3.4 μm feature is very weak or absent in Elias 25, notwithstanding the arguments presented in § 1 that this object samples an environment apparently conducive to the formation of one of the proposed carriers. We now consider the significance of our result in terms of the production of carbonaceous dust in the ISM.

The degree of visual extinction along the line of sight to Elias 25 ($A_V \approx 12.5$) is a measure of the total dust column. Some of this extinction must arise in ice-mantled dust that presumably survives in the densest clump(s) along the line of sight. However, the extinction toward Elias 25 is similar to the threshold visual extinction for detection of the 3.1 μm ice feature in the ρ Oph cloud ($A_0 \sim 10$–15; Tanaka et al. 1990). The threshold extinction is higher in ρ Oph than in dark clouds (such as Taurus) that lack embedded early-type stars (Tanaka et al. 1990; Whittet et al. 2001a), consistent with the hypothesis that ice mantles have been processed or sublimated in regions where the UV field permeates. The majority of the extinction along the line of sight to Elias 25 is thus expected to arise in grains that (currently) lack ice mantles but that might carry their photolyzed residues.

We assume the ratio $\tau_{3.4}/A_V$ to be a measure of the abundance of the agent responsible for the 3.4 μm C—H feature. Our upper limit for $\tau_{3.4}$ in Elias 25 implies a limiting value of $\tau_{3.4}/A_V < 0.0008$. The total extinction toward Elias 25 is similar to that toward Cyg OB2 No. 12 ($A_V \approx 10.2$; Adamson, Whittet, & Duley 1990), suggesting comparable contributions from dust lacking ice mantles in the two lines of sight. For the latter object, $\tau_{3.4} \approx 0.04$ (Whittet et al. 1997), and thus $\tau_{3.4}/A_V \approx 0.004$. Hence, the feature seen in Cyg OB2 No. 12 (see Fig. 3*b*) is a factor of about 4 stronger than the upper limit in Elias 25. We conclude that the carrier is substantially *depleted* in the line of sight to Elias 25 compared with the diffuse ISM.

The fact that the carrier is depleted toward Elias 25 implies *destruction or modification* of the carrier, not merely a failure to produce. If organic mantles are being formed, they must be rapidly removed or dehydrogenated. Dehydrogenation naturally reduces the strength of the 3.4 μm

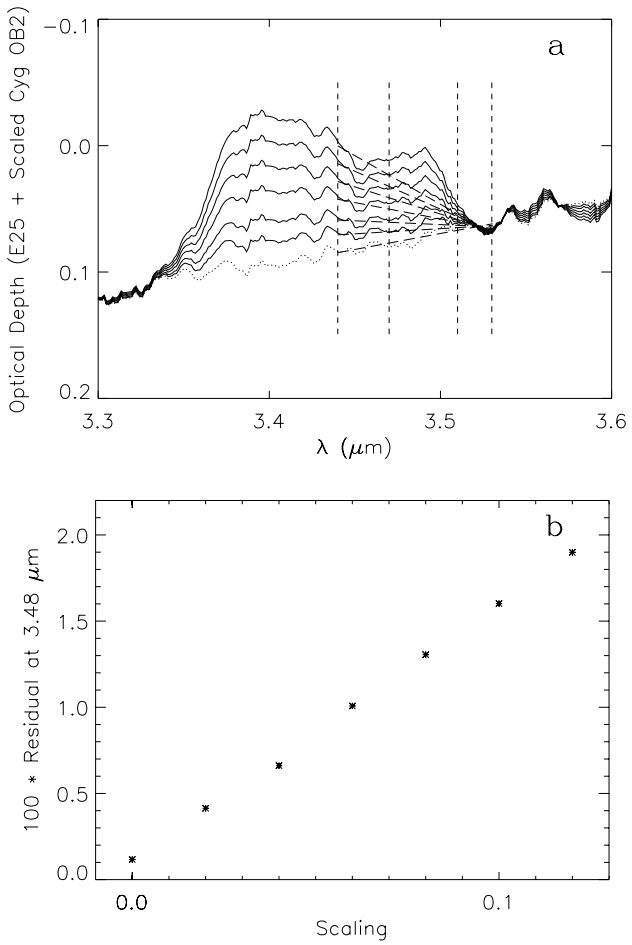


FIG. 4.—(*a*) Composite spectra of Elias 25 and Cyg OB2 No. 12. The dotted curve is the optical depth of Elias 25 alone. The first solid curve above the dotted curve represents the Elias 25 spectrum minus the Cyg OB2 No. 12 spectrum, with the latter scaled to give a peak optical depth of 0.02 in the 3.4 μm feature; subsequent curves have scaling 0.04, 0.06, ..., 0.12. The strength of the sub-peak at 3.48 μm is estimated by fitting a linear baseline to the two peripheral regions indicated by the vertical dashed lines. (*b*) Residual at 3.48 μm relative to the linear baseline in Fig. 4*a* plotted against 3.4 μm scale factor.

absorption per unit dust column. In the diffuse ISM, a balance is expected between hydrogenation and dehydrogenation (Muñoz Caro et al. 2001); but in dense clouds, where most of the hydrogen is molecular, this balance may be disturbed in favor of destruction of the carrier. The chemical processes that lead to ice formation on grain surfaces may scavenge hydrogen (Grishko & Duley 2000), but our results imply that the carrier is also depleted in regions that lack ice mantles. The UV radiation that photolyzes the mantles may also be responsible for dehydrogenating the products of photolysis (see Mennella et al. 2002).

We conclude that organic refractory matter is probably not an important constituent of dust in the general interstellar medium. This conclusion is consistent with other evidence: as noted in § 1, laboratory-synthesized ORM possesses features at other wavelengths in addition to the C—H feature at 3.4 μm, notably the carbonyl feature near 6 μm, and the lack of such features in the spectrum of diffuse ISM dust indicates that any organic component must be predominantly hydrocarbon (Pendleton & Allamandola 2002). Carbon-rich stellar outflows provide one possible source of carbon grains, and subsequent hydrogenation in the ISM may lead to production of the 3.4 μm feature (Chiar et al. 1998; Mennella et al. 1999, 2002). Photolysis of icy mantles might, nevertheless, be an important source of carbonaceous grain material in the general ISM if the radiative environment that drives formation quickly reduces organics to amorphous carbon lacking in C—H and C═O bonds. In this scenario, organic refractory matter would represent an important *transitional* phase in the evolution of carbonaceous dust around newly formed stars (Gibb & Whittet 2002). Finally, we note that the absence of polarization excess in the 3.4 μm feature observed in two lines of sight (Adamson et al. 1999; Ishii et al. 2002) suggests that the carrier resides in very small particles that fail to align, rather than as a coating on the larger aligned grains responsible for visual extinction and polarization; however, further observations are needed to confirm this (see Li & Greenberg 2002).

We thank Paul Hirst and the UKIRT staff for obtaining the data on Elias 25 during a service run. This work is supported by the NASA Exobiology and Long-Term Space Astrophysics programs under grants NAG5-7598, NAG5-7884 and NAG5-9148. J. E. C. is supported by NASA's Long-Term Space Astrophysics program under grant 399-20-61-02. The paper benefited from comments by an anonymous referee.

REFERENCES

Adamson, A. J., Whittet, D. C. B., Chrysostomou, A., Hough, J. H., Aitken, D. K., Wright, G., & Roche, P. F. 1999, ApJ, 512, 224
Adamson, A. J., Whittet, D. C. B., & Duley, W. W. 1990, MNRAS, 243, 400
Allamandola, L. J., Sandford, S. A., Tielens, A. G. G. M., & Herbst, T. M. 1992, ApJ, 399, 134
Bohlin, R. C., & Savage, B. D. 1981, ApJ, 249, 109
Boogert, A. C. A., et al. 2000, A&A, 360, 683
———. 2002, ApJ, 570, 708
Briggs, R., et al. 1992, Origins Life Evol. Biosphere, 22, 287
Brooke, T. Y., Sellgren, K., & Geballe, T. R. 1999, ApJ, 517, 883
Brooke, T. Y., Sellgren, K., & Smith, R. G. 1996, ApJ, 459, 209
Cecchi-Pestellini, C., Aiello, S., & Barsella, B. 1995, ApJS, 100, 187
Chiar, J. E., Adamson, A. J., & Whittet, D. C. B. 1996, ApJ, 472, 665
Chiar, J. E., Pendleton, Y. J., Geballe, T. R., & Tielens, A. G. G. M. 1998, ApJ, 507, 281
de Vries, M. S., et al. 1993, Geochim. Cosmochim. Acta, 57, 933
Elias, J. H. 1978, ApJ, 224, 453
Gibb, E. L., & Whittet, D. C. B. 2002, ApJ, 566, L113
Grasdalen, G. L., Strom, K. M., & Strom, S. E. 1973, ApJ, 184, L53
Greenberg, J. M., Li, A., Mendoza-Gómez, C. X., Schutte, W. A., Gerakines, P. A., & de Groot, M. 1995, ApJ, 455, L177
Grishko, V. I., & Duley, W. W. 2000, ApJ, 543, L85
Hong, S. S., & Greenberg, J. M. 1980, A&A, 88, 194
Ishii, M., Nagata, T., Chrysostomou, A., & Hough, J. H. 2002, AJ, 124, 2790
Jenniskens, P., Baratta, G. A., Kouchi, A., de Groot, M. S., Greenberg, J. M., & Strazzulla, G. 1993, A&A, 273, 583
Jura, M. 1980, ApJ, 235, 63
Li, A., & Greenberg, J. M. 1997, A&A, 323, 566
———. 2002, ApJ, 577, 789
Liseau, R., et al. 1999, A&A, 344, 342
Mennella, V., Brucato, J. R., Colangeli, L., & Palumbo, P. 1999, ApJ, 524, L71
———. 2002, ApJ, 569, 531
Muñoz Caro, G. M., Ruiterkamp, R., Schutte, W. A., Greenberg, J. M., & Mennella, V. 2001, A&A, 367, 347
Pendleton, Y. J., & Allamandola, L. J. 2002, ApJS, 138, 75
Sandford, S. A., Allamandola, L. J., Tielens, A. G. G. M., Sellgren, K., Tapia, M., & Pendleton, Y. 1991, ApJ, 371, 607

Schnaiter, M., Henning, T., Mutschke, H., Kohn, B., Ehbrecht, M., & Huisken, F. 1999, ApJ, 519, 687
Smith, R. G., Sellgren, K., & Tokunaga, A. T. 1989, ApJ, 344, 413
Strazzulla, G., & Baratta, G. A. 1992, A&A, 266, 434
Tanaka, M., Sato, S., Nagata, T., & Yamamoto, T. 1990, ApJ, 352, 724
Tielens, A. G. G. M., McKee, C. F., Seab, C. G., & Hollenbach, D. J. 1994, ApJ, 431, 321
Vrba, F. J., Coyne, G. V., & Tapia, S. 1993, AJ, 105, 1010
Vrba, F. J., Strom, K. M., Strom, S. E., & Grasdalen, G. L. 1975, ApJ, 197, 77
Whittet, D. C. B., Gerakines, P. A., Hough, J. H., & Shenoy, S. S. 2001a, ApJ, 547, 872
Whittet, D. C. B., Martin, P. G., Hough, J. H., Rouse, M. F., Bailey, J. A., & Axon, D. J. 1992, ApJ, 386, 562
Whittet, D. C. B., Pendleton, Y. J., Gibb, E. L., Boogert, A. C. A., Chiar, J. E., & Nummelin, A. 2001b, ApJ, 550, 793
Whittet, D. C. B., et al. 1997, ApJ, 490, 729